AIR FLOW CHARACTERISTICS OF STAGGERED WING-SHAPED TUBE BUNDLE AT DIFFERENT ANGLES OF ATTACK[*].

Sayed Ahmed E. Sayed, Emad Z. Ibrahiem,
Osama M. Mesalhy, Mohamed A. Abdulatief[+]

Mech. Power Eng. Dept. , Faculty of Engineering, Zagazig Univ., Egypt

ABSTRACT

An experimental and numerical study has been conducted to clarify fluid flow characteristics and pressure drop distributions of a cross-flow heat exchanger employing staggered wing-shaped tubes at different angles of attack. The water-side Re_w and the air-side Re_a were at 5×10^2 and at from 1.8×10^3 to 9.7×10^3, respectively. Three cases of the tubes arrangements with various angles of attack, row angles of attack and $90°$ cone angles were employed at the considered Re_a range. Correlation of pressure drop coefficient P_{dc} in terms of Re_a, design parameters for the studied cases were presented. The flow pattern around the staggered wing-shaped tubes bundle were predicted using the commercial CFD FLUENT 6.3.26 software package. Results indicated that the values of P_{dc} increased with the angle of attack from $0°$ to $45°$, while the opposite was true for angles of attack from $135°$ to $180°$. Comparisons between the experimental and numerical results of the present study and those obtained by similar previous studies showed good agreements.

KEY WORDS: Wing-Shaped Tubes Bundle, Cross-Flow Cooling, Staggered Arrangement, and CFD.

**FLUX D'AIR CARACTERISTIQUES DES STAGGERED AILE EN FORME
Tubes Bundle À DIFFÉRENTS ANGLES D'ATTAQUE *.**

RÉSUMÉ

Une étude expérimentale et numérique a été menée afin de clarifier les caractéristiques d'écoulement de fluide et les distributions de chute de pression d'un échangeur de chaleur à flux croisés en utilisant des tubes en forme d'ailes décalées à différents angles d'attaque . Bord de l'eau et l'air Rew côté Rea sont à 5 x 102 et à partir de 1,8 x 103 à 9,7 x 103 , respectivement . Trois cas des arrangements de tubes avec différents angles d'attaque , les angles de lignes d'attaque et 90 ° des angles de cône ont été employés à la gamme Rea considéré . Corrélation du coefficient de perte de charge Pdc en termes de Rea , paramètres de conception pour les cas étudiés ont été présentés . Le modèle d'écoulement autour du quinconce des tubes en forme d'ailes faisceau ont été prédits à l'aide du logiciel 6.3.26 commercial CFD FLUENT . Les résultats ont indiqué que les valeurs de Pdc augmenté avec l'angle d'attaque de 0 ° à 45 ° , tandis que l'inverse était vrai pour les angles d' attaque de 135 ° à 180 ° . Les comparaisons entre les résultats expérimentaux et numériques de la présente étude et ceux obtenus par des études antérieures ont montré de bons accords similaires .

MOTS CLÉS: Wing- forme Tubes Bundle , Croix - flux de refroidissement , disposés en quinconce , et CFD .

AIR FLOW CHARACTERISTICS OF STAGGERED WING-SHAPED
TUBE BUNDLE AT DIFFERENT ANGLES OF ATTACK.
Sayed, Ibrahiem, Mesalhy, Abdulatief

EIJEST

1. INTRODUCTION

Heat exchangers have been playing a vital role in energy applications for a long time. Economical and environmental issues progressively place the needs for compactness and performance improvement of such systems. In this regard, tubes of various shapes and arrangements have been studied experimentally and numerically.

Zukauskas and Ulinskas [1] suggested correlations for heat transfer and pressure drop for in-line and staggered banks of circular tubes. Their study covered the range of $1 \leq Re_a \leq 2 \times 10^6$, and $0.7 \leq Pr \leq 500$, as well as a wide range of relative transverse and longitudinal pitches. They suggested an efficiency factor for the evaluation of heat transfer surfaces efficiency in further improvement of heat exchangers constructions.
Comparisons of circular and elliptical tubes as the essential elements of heat exchangers have been reported in several studies, for example, Brauer [2] reported 18 % of relative reduction in the pressure drop for elliptical tubes compared to circular ones. Horvat et al. [3] studied the transient heat transfer and fluid flow for circular, elliptical, and wing-shaped tubes with the same cross sections. Comparing the three types of tubes, they reported that the values of the average drag coefficient were lower for the ellipsoidal and the wing-shaped tubes than those for the cylindrical ones.

The effects of cylinders spacing and angles of attack on the drag coefficient for elliptical tubes in tandem arrangement were investigated by Nishiyama et al. [4]. They found that the angle of attack, as well as, the cylinders spacing influenced the drag coefficients. They concluded that the cylinders spacing and the angles of attack should be arranged as small as possible to minimize the drag and to achieve compactness of the system. Harris and Goldschmidt [5] investigated the effects of the variation of the tube axis ratios and angles of attack on the drag coefficient for Rea ranging from 7.4×10^3 to 7.4×10^4. Rea was based on the length of the major axis. They concluded that an axis ratio of 0.30 or less must be achieved. Ibrahim and Gomma [6] have performed experimental and numerical studies of the turbulent flow over bundle of elliptical tubes. Their investigation covered a range of Rea from 5.6×10^3 to 40×10^3 with four axis ratios considered (0.25, 0.33, 0.5 and 1) and the flow angles of attack were varied from $0°$ to $150°$. Their

results showed that the best and worst flow angles of attack were $0°$ and $90°$, respectively for fixed pumping power. Ibrahim et al.[7], conducted an experimental investigation of the performance of a bundle of semi-circular tubes. Rea was ranged from 2×10^4 to 16.5×10^4, the angles of attack were varied from $0°$ to $270°$ and the relative longitudinal pitch SL/d was at 1.35 and 2.69, while the relative transverse pitch was kept at ST/d=1.35. They concluded that the best and worst angles of attack were $270°$ and $0°$, respectively.

Sayed Ahmed et al. [8], experimentally and numerically, studied the flow and heat transfer characteristics of a cross flow heat exchanger employing staggered wing-shaped tubes with zero angle of attack. Hot air was forced to flow over the external surfaces of the tubes and exchanged heat with the cold water flowing inside. The results indicated that, the bundle of wing-shaped tubes has better performance over other bundles for similar parameters and conditions.

It can be noticed from the above discussion, to the author's knowledge, that the available data on forced convection for wing-shaped tubes are not enough. Therefore, the aim of the present study was to investigate the air flow characteristics and pressure contours through the wing-shaped tubes bundle in cross-flow with various angles of attack. To achieve these goals, experimental and numerical studies have been conducted. Three cases of the tubes arrangements, with various angles of attack ($\theta_{1,2,3}$), row angles of attack (θ_i) and $90°$ cone angles (ϕ) were employed with different Rea.

2. EXPERIMENTAL DETAILS AND DATA COLLECTION

The experiments were conducted in an open-suction-type wind tunnel of 2780 mm length, as shown in Fig.(1). The tunnel is capable of producing an air velocity up to 7.3 m/s. Plexiglas test section of (305×305) mm^2, and 780 mm long is mounted in the middle of the wind tunnel. The cross-sectional dimensions of wing-shaped tube, drawn from 1 mm thick, 22.5 mm outer diameter circular copper tube with 305 mm long, is shown in Fig. (2a). The tested tube bundle, shown in Fig.(2b), consists of 22 wing-shaped tubes distributed through three successive rows in addition to four half dummy ones. The tubes of the bundle could be fixed in the test section with a special

mechanism having the capability of changing the flow angle of attack ($\theta_{1,2,3}$), while the longitudinal (S_L) and transverse (S_T) tube-pitches of 37 mm were kept constant. The flow angle of attack, as illustrated in Fig.(3), could be adjusted by turning the tube, clockwise, around a vertical axis at the center of a flat surface using a protractor mechanism. If all tubes in the three rows adjusted at the same angle, this will be denoted as $\theta_{1,2,3}$. When θ was kept constant for all tubes of the same row it denoted as the row flow angle of attack (θ_i), where i = 1, 2 and/or 3. The flow angle of attack created between every two neighboring tubes, in the same row, by turning one of them 45° clockwise and 45° counter clockwise for the other one simultaneously, thus yielding 90°, will be denoted, hereafter, as the cone angle (ϕ_i), Fig.(4). Three cases of the tubes arrangements were considered. Table (1) shows the angles of arrangements of the considered cases. Air was heated via 4 kW electrical heater installed in the entrance of the wind tunnel. Air at 56.5±1.5 $^\circ$C dry bulb and 26±1.5°C wet bulb temperature entered the test section and passed over the tubes bundle. A 134A refrigeration system was employed for keeping the, flowing inside tubes, water at 10.8±1.5 $^\circ$C.

2.1 Measuring Techniques

T-type thermocouples were used to measure the temperatures. Water flow inlet, T_{wi} and exit, T_{we} temperatures, were measured by means of a single point measurement. Air flow inlet, T_{ai} and exit, T_{ae} average temperatures, were measured via 8 thermocouples arranged uniformly on two grids at the entrance and the exit of the test section. The wet bulb temperatures at inlet and exit were measured by using alcohol thermometer with wet wick surrounded bulb. The surface temperatures of the tubes, T_s were measured by attaching 2 thermocouple probes on the outer surface of each tube of the tested bundle. The average temperature of every tube was taking to be as the average of the two probes attached to its surface. A hand-held digital thermometer with an uncertainty of ±0.2 $^\circ$C with ±0.1 $^\circ$C sensitivity was used to record the temperatures. The airflow pressure drop (ΔP_a) caused by the studied bundle was measured via an electrical micro-manometer of ± 0.1 mm H_2O accuracy of full scale, (manufactured by Furness controls company, model FC 001, and serial number (FN 2561), which was connected to 4 pressure taps as depicted in Fig.(7).

Four different cold-water mass flow rates (m_w) of 0.205, 0.26, 0.35 and 0.43 kg/s were considered. The water flow rates were measured, at the beginning of each test run, using bucket stopwatch method. The mean velocity (V_{ai}) of the air flow was varied from 1.33 to 7 m/s, yielding Re_a from 1.8×10^3 to 9.7×10^3 while $Re_w = 5 \times 10^2$. The air velocities for subsequent experiments were measured at a single point around the entrance-center of the test section with a 3 mm Pitot static tube using the same electrical micro-manometer as used in the pressure drop measurement. All of the experiments were conducted at the same inlet conditions with Re_a and Re_w, based on the tube equivalent diameter D_{eq}.

2.2 Data Reduction and Flow Considerations

Steady state flow conditions were achieved during the experiments. The fluid properties, for both air and water, were determined from tables given by Cengel [9].

Table 1: Angles of Arrangements of Considered Cases.

Case no.	Angle(degree)	
	Experimental	Numerical
Case (1)	$\theta_{1,2,3} \rightarrow (0°, 45°, 135°, 180°, 225°, 315°)$	$\theta_{1,2,3} \rightarrow (0°, 30°, 45°, 135°, 150°, 180°, 210°, 225°, 315°, 330°)$
Case (2)	$[(\theta_1 = 45°, \theta_2 = 0°, \theta_3 = 45°)]$ $[(\theta_1 = 45°, \theta_2 = 0°, \theta_3 = 0°)]$	$[(\theta_1 = 45°, \theta_2 = 0°, \theta_3 = 45°)]$ $[(\theta_1 = 0°, \theta_2 = 45°, \theta_3 = 45°)]$ $[(\theta_1 = 45°, \theta_2 = 45°, \theta_3 = 0°)]$ $[(\theta_1 = 45°, \theta_2 = 0°, \theta_3 = 0°)]$ $[(\theta_1 = 0°, \theta_2 = 45°, \theta_3 = 0°)]$ $[(\theta_1 = 0°, \theta_2 = 0°, \theta_3 = 45°)]$
Case (3)	$\phi_1 = 90°, \phi_2 = 90°, \phi_3 = 90°$ $\phi_1 = 90°, \theta_2 = 0°, \phi_3 = 90°$ $\phi_1 = 90°, \theta_2 = 0°, \theta_3 = 0°$	$\phi_1 = 90°, \phi_2 = 90°, \phi_3 = 90°$ $\phi_1 = 90°, \theta_2 = 0°, \phi_3 = 90°$ $\phi_1 = 90°, \theta_2 = 0°, \theta_3 = 0°$

AIR FLOW CHARACTERISTICS OF STAGGERED WING-SHAPED TUBE BUNDLE AT DIFFERENT ANGLES OF ATTACK.
Sayed, Ibrahiem, Mesalhy, Abdulatief

EIJEST

If not mentioned otherwise, all the thermo-physical properties for air were evaluated at the air film temperature. Considering a linear variation of temperature between the outer surface of the tubes and the approaching air, the air film temperature was deduced as follows: $\left(T_{af} = \dfrac{T_{ai} + T_s}{2}\right)$, while for water at bulk temperature, T_{wb}.

Mean inlet air velocity was calculated from the measured data by the standard Pitot tube through the following relationship:

$$V_{ai} = \sqrt{2g\left(\frac{\rho_w}{\rho_{a,f}}\right)\Delta h_{dyn}}, \quad (m/s) \tag{1}$$

where, Δh_{dyn} is the head difference between the total and static pressure heads through Pitot tube, m H_2O,

while ρ_w and $\rho_{a,f}$ are the average densities for water and air respectively, kg/m^3. The pressure drop coefficient, P_{dc}, as defined below in Eq. (2), represents the ratio of the total pressure drop of the moving air over the tube bundle to its dynamic pressure

$$P_{dc} = \frac{2\Delta p_a}{\rho_{af}\, V_{ai}^{\,2}} \tag{2}$$

where, the pressure drop through the tube bundle, Δp_a was measured by the electrical micro-manometer via pressure taps, and ρ_{af} is the air film density.

The Reynolds number, Re_a was given by:

$$Re_a = \frac{\rho_{af} V_{ai} D_{eq}}{\mu_{af}} \tag{3}$$

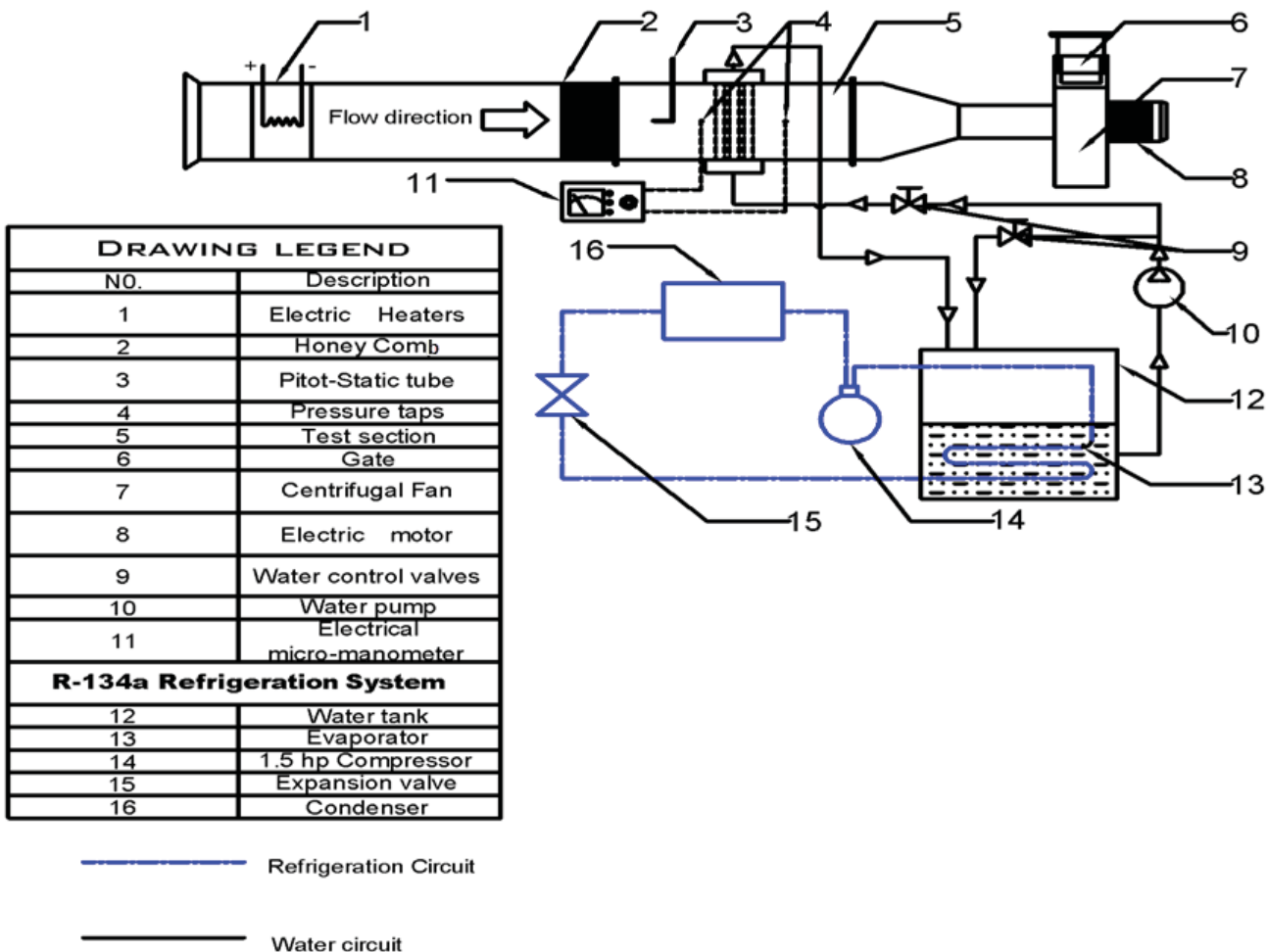where, D_{eq} is the outer equivalent diameter of the tube.

DRAWING LEGEND	
NO.	Description
1	Electric Heaters
2	Honey Comb
3	Pitot-Static tube
4	Pressure taps
5	Test section
6	Gate
7	Centrifugal Fan
8	Electric motor
9	Water control valves
10	Water pump
11	Electrical micro-manometer
R-134a Refrigeration System	
12	Water tank
13	Evaporator
14	1.5 hp Compressor
15	Expansion valve
16	Condenser

Refrigeration Circuit

Water circuit

EIJEST

Figure 1 : Schematic Drawing of Experimental Setup
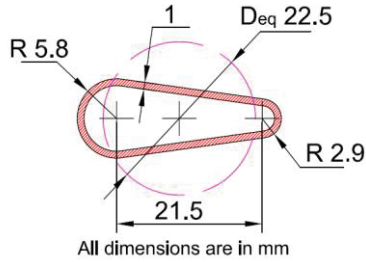
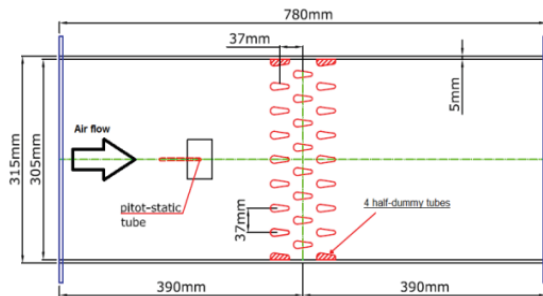**Figure 2a :** Wing- shaped Tube Cross Sectiona.

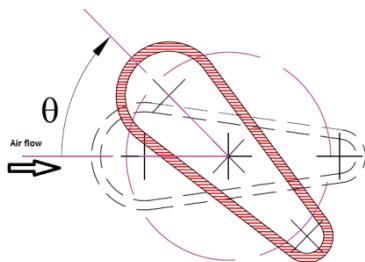**Figure 2b :** Schematic Plane of The test Section, $\theta_{1,2,3} = 0^{\circ}$, (Case 1).
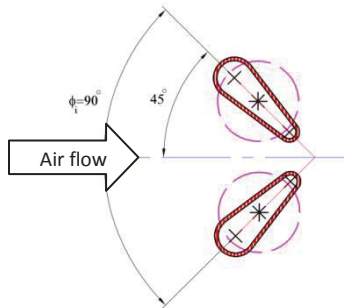
Figure 3 : Adjusting The Flow Attack Angle.
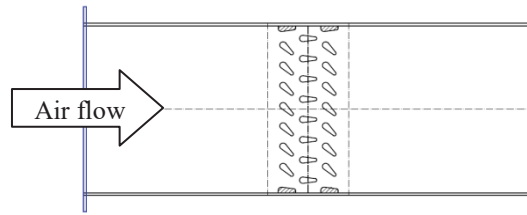
Figure 4: The tubes Cone Angle.

Figure 5: Schematic Drawing of Wing-Shaped Tubes Bundle for Case (2), [(θ_1=45°,θ_2=0°,θ_3=45°)].
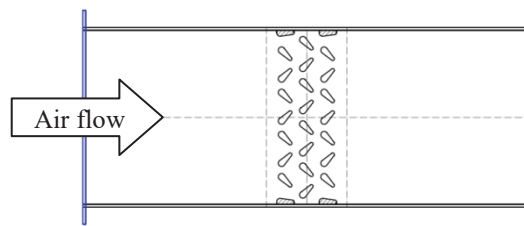
Figure 6: Schematic Drawing of Wing-Shaped Tubes Bundle for Case (3), [(ϕ_1=90°,ϕ_2=90°,ϕ_3=90°)].
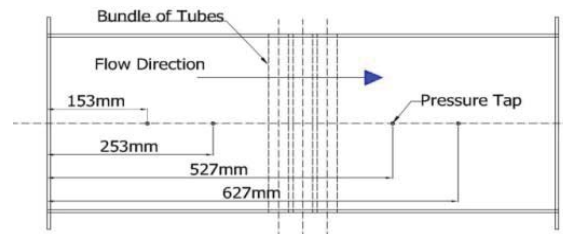
Figure 7 : Locations of Pressure Taps.

2.3   Measurement Uncertainties

Generally, the accuracy of the experimental results depends upon the accuracy of the individual measuring instruments and the manufacture accuracy of the wing-shaped tubes. Also, the accuracy of an instrument is limited by its minimum division (its sensitivity). The experimental error analysis indicated the implication of error of the measured parameters on the uncertainty of the results. The maximum errors in measuring parameters are: ± 1.053%, ± 4.2%, and 3.4% for temperature, pressure drop across the heat exchanger and dynamic pressure at inlet, respectively. However, the maximum uncertainties of the results that have been obtained from the measured parameters

AIR FLOW CHARACTERISTICS OF STAGGERED WING-SHAPED TUBE BUNDLE AT DIFFERENT ANGLES OF ATTACK.
Sayed, Ibrahiem, Mesalhy, Abdulatief

EIJEST

for (V_{ai}), (V_{wi}), (m_a), ($FR_{a,i}$), (Q_a), (h), (St), Re_a, (P_{dc}), pumping power and (ε) are summarized in table (2).

3. NUMERICAL INVESTIGATION

3.1. Problem Description and Boundary Conditions

Since, the tube length is much greater than its equivalent diameter, the flow across the tube bundle is considered two-dimensional. The geometry of the numerical model includes entrance section, tube bundle section, and exit section beside the boundary conditions, are shown in Fig.(8). The numerical solution is carried out by solving the governing equations of mass, momentum and energy under the following assumptions; the flow is incompressible, steady and turbulent, fluid properties are constant, the effect of buoyancy force and radiation are neglected, Fluent [10]:

$$\frac{\partial}{\partial x_i}(\rho V_i) = 0.0 \tag{4}$$

$$\frac{\partial}{\partial x_j}(\rho V_i V_j) = -\frac{\partial p}{\partial x_i} + \frac{\partial \tau_{ij}}{\partial x_j} \tag{5}$$

$$\frac{\partial}{\partial x_i}[V_i(\rho E + p)] = \frac{\partial}{\partial x_i}\left(k\frac{\partial T}{\partial x_i}\right) \tag{6}$$

where, i: is a tensor indicating 1 and 2, τ_{ij} is the viscous stress tensor, and k is the fluid effective thermal conductivity

Commercial CFD software FLUENT 6.3.26 was used to solve the governing equations. RNG κ−ε turbulent model is utilized to solve the complicated turbulent thermal flow field with Enhanced Wall Function approach in the near-wall regions to fit the wall boundary conditions, Fluent [10].
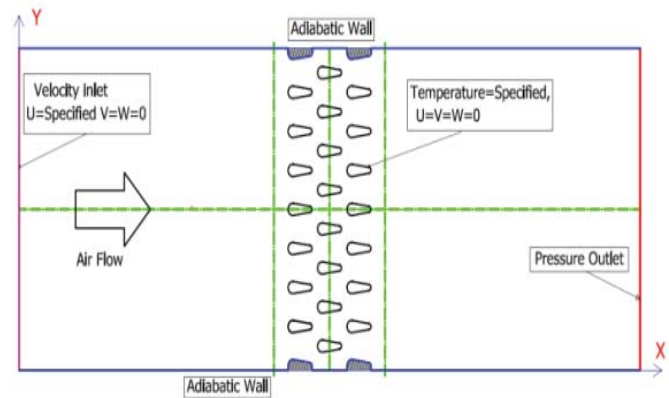

Figure 8 : Boundary Conditions.

3.2. Mesh Generation and Discretization

The geometry and mesh of the computational model that described in the previous section were generated separately using GAMBIT 2.4.6. Quad/Map, Tri/Pave and boundary layer meshing scheme was used in the present study with refining the mesh near walls and beside sharp edges. Figures (9) and (10) show the configuration of the computational domain mesh. A finite volume discretization method using second order upwind schema for momentum, turbulent kinetic energy, and turbulent dissipation rate was applied, besides using simple-based solution algorithm of the velocity–pressure coupling with a segregated solver. The solution was considered converged when the scaled residual of the energy equation reaches 10^{-7} and the scaled residuals of other equations reach 10^{-4}.
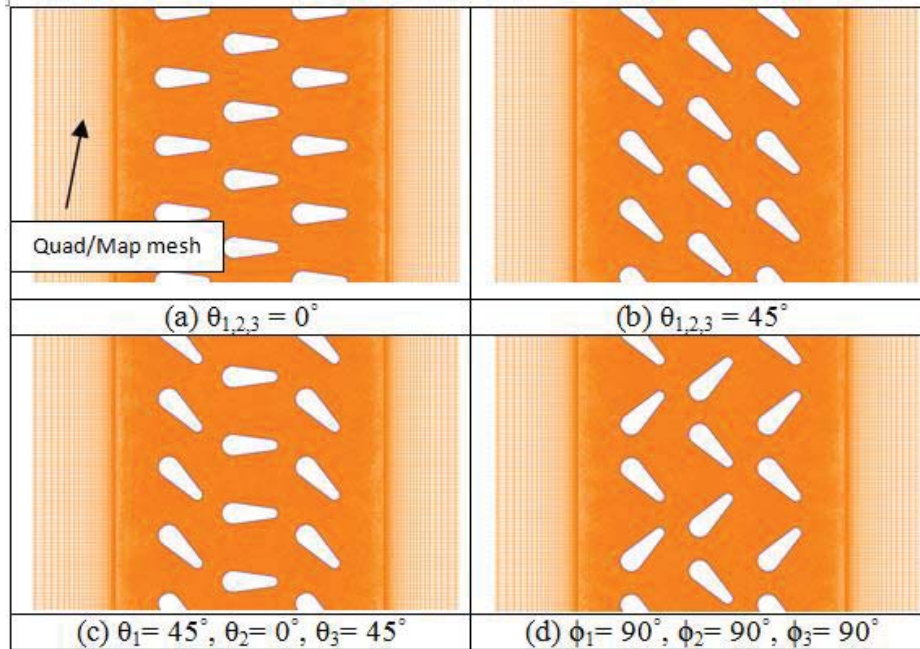
Table 2: Uncertainties of Compound Variables

Compound Variable	Uncertainty (± %)
Air Flow Velocity at the Inlet, $V_{a,i}$	1.71
Water Flow Velocity at the Inlet, $V_{w,i}$	1.5
Air mass Flow Rate, m_a	1.746
Air volume Flow Rate, $FR_{a,i}$	1.71
Heat Transfer Rate at the Air Side, Q_a	1.82
Heat Transfer Coefficient at the Air Side, h_a	2.13
Stanton Number at the Air Side, St_a	2.78
Air Flow Reynolds Number, Re_a	1.83
Pressure Drop Coefficient at the Air Side, P_{dc}	5.44
Heat transfer per unit pumping power, ε	4.27
The pumping power	4.53

EIJEST

Figure 9 : Mesh Configurations for The domain of The Tubes Bundle.
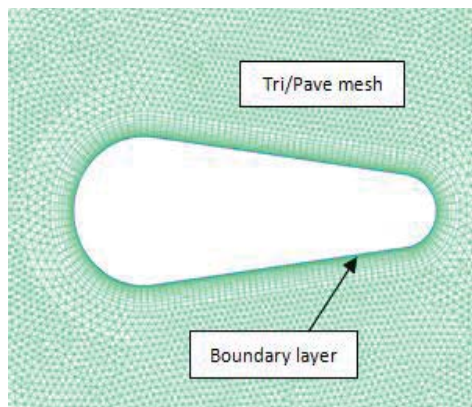

Figure 10 : Mesh Details Around The Wing-Shaped Tube.

4. RESULTS AND DISCUSSION

4.1 Characteristics of Air Flow

Flow path lines and contours across the wing-shaped tubes of the studied bundle arranged for different angles of attack are illustrated in Figs.(11 and 12). where Fig.11 (a, b, c & d) presents the illustration for case 1. while Fig.11 (e & f) and (g & h) presents the arrangements for the second and third cases, respectively.

As shown in Fig.(11.a), for $\theta_{1,2,3} = 0°$ and $Re_a = 1.8 \times 10^3$ there are three flow separation-zones two at the lateral and one at the rear surfaces of the tubes. Flow separations are occurred, as a result of travelling of the boundary layer far enough against an adverse pressure gradient, that makes the velocity of the boundary layer falls, almost, to zero. On the other hand, flow separation can be occurred as a result of the increase of the pressure drag caused by the pressure differential of the flowing air between the frontal and rear surfaces of the tube.

It is seen from Fig.(11.b) that with increasing the Rea the eddies and vortices at lateral tube surfaces are disappeared, while they existed only at its rear surface. This is due to, the fact that for high Rea, the flow becomes more energetic enabling the boundary layer to travel further along with the tube surface before separation occurs resulting, only, in a narrower wake at the rear surface of the tube.

For the arrangement of $\theta_{1,2,3} = 45°$, as shown in Fig.(11.c), at low Re_a, the separation-zone areas at the down-stream lateral surfaces of the tubes in the first row increased due to the bluff nature of the first row with respect to the flow direction. The first row, also, directs the flow passing through the successive rows so, the separation disappeared in the second and third rows. For high Rea, as shown in Fig.(11.d), separation intensity increased after the first row and at the down-stream lateral surfaces of the tubes in the second row comparing with those of Fig.(11.c).

For the arrangement of $(\theta_1=45°, \theta_2=0°, \theta_3=45°)$ at low Rea, as shown in Fig.(11.e), separation-zone areas are occurred at the down-stream lateral surfaces of the

AIR FLOW CHARACTERISTICS OF STAGGERED WING-SHAPED TUBE BUNDLE AT DIFFERENT ANGLES OF ATTACK.
Sayed, Ibrahiem, Mesalhy, Abdulatief

EIJEST

tubes in the first and third rows. For the second row $(\theta_2 = 0^\circ)$ separation areas are occurred at the opposite lateral sides of the tubes row surfaces (facing downward in the figure). In general, all separation areas are occurred due to the effect of the adverse and favorable pressure gradients of the flow when crossing the tubes at various orientations. On the other hand, for high Re_a, as shown in Fig.(11.f), separations and secondary-flows intensity are occurred, mainly, at the down-stream lateral surfaces of the tubes in the first row due to the high momentum mixing in the main flow.

As shown in Fig.(11.g&h), for the arrangement with cone angle $(\phi = 90^\circ)$ for the all rows. Convergent and divergent configurations were created between every two neighboring tubes surfaces of every row. The separation areas and secondary-flows intensity are occurred at all the down-stream lateral surfaces of the tubes due to the favorable and adverse pressure gradients caused by the flow accelerations and decelerations, respectively.

As seen in Fig.(12) for $(\theta_{1,2,3} = 0^\circ)$, the airflow is strongly accelerated in the passages between tubes. For angle of attack $\theta_{1,2,3} = 45°$ the air flow acceleration between tubes seems to be more than that for case $\theta_{1,2,3} = 0°$. This happens due to the fact that the passages between every two adjacent tubes in every row serve as stream jets, thus possessing, a relatively, higher amount of momentum.

It is, also, noticed that for the arrangements of $(\theta_1=45^\circ, \theta_2=0^\circ, \theta_3=45^\circ)$ and $(\phi_1=90^\circ, \phi_2=90^\circ, \phi_3=90^\circ)$, the level of turbulence and formation of vortices through the passages of the bundle were increased.

Figure (13) presents the turbulent kinetic energy contours through the wing-shaped tubes of the bundle for both low and high Re_a, which is defined as the mean kinetic energy per unit mass associated with eddies in turbulent flow. Physically, the turbulent kinetic energy is characterized via root-mean-square (RMS) produced by fluid shear, friction and buoyancy, or through external forcing at low-frequency eddie scales (integral scale). Turbulence kinetic energy is transferred down the turbulence energy cascade, and dissipated by viscous forces at the Kolmogorov scale (Smallest scales in the spectrum that form the viscous sub-layer range). It is found that the turbulent kinetic energy is larger in magnitude in the case of the higher Re_a It is, also, seen from the figure that there are a direct proportionality between Re_a. and the values of turbulent kinetic energy (k)

but the numerical results show that the values of (k) at the exit section of the bundle are always greater than those at the inlet one for the considered Re_a range, so the bundle works as a turbulence generator which leads to an increase in the heat transfer between tubes and flowing air. On the other hand it is found that the maximum values of the turbulent kinetic energy are taken place at the arrangement of $(\phi_1=90^\circ, \phi_2=90^\circ, \phi_3=90^\circ)$, while the minimum values are occurred at $\theta_{1,2,3} = 0^\circ$. This, in turn, increases the pressure drop.

4.2 Air Flow Pressure Drop Through The Bundle

Figure (14) demonstrates the static pressure contours through the bundle. It can be seen that the pressure has the highest values at the stagnation point on the frontal portion of each tube for $\theta_{1,2,3} = 0^\circ$, this is because the flow velocity tends to be zero at this point. As the flow passes over the tube surface the pressure decreases until reaching the lowest value at lateral surface. The static pressure drop for the bundle with $\theta_{1,2,3}=45^\circ$ is higher than that with $\theta_{1,2,3}=0^\circ$.

This is due to the shifting of the stagnation point from the frontal portion at $\theta_{1,2,3} = 0^\circ$ to the up-stream lateral surface of each tube. The pressure decreases as the air is flowing over the tubes surfaces. For the arrangement of $(\phi_1=90^\circ, \phi_2=90^\circ, \phi_3=90^\circ)$ with $Re_a = 9.7$ x 10^3 the pressure drop has the maximum value, because flowing through the convergent and divergent passages between the tubes surfaces.

4.2.1 First case for numerical and experimental study

Figure (15) shows the validation of numerical and experimental P_{dc} versus Re_a at different $\theta_{1,2,3}$. It is seen from the figure that P_{dc} decreases with the increase of Re_a for all arrangements at a certain $\theta_{1,2,3}$. Maximum and minimum values of P_{dc} are occurred for arrangements of $\theta_{1,2,3} = 45^\circ, 135^\circ$ at $Re_a = 1.8$ x 10^3 and for $\theta_{1,2,3} = 0^\circ, 180^\circ$ at $Re_a = 9.7$ x 10^3, respectively. The values of P_{dc} for $\theta_{1,2,3} = 135^\circ$ are higher than these of 45° by about 6 %, while they are higher by about 32 % for $\theta_{1,2,3} = 180^\circ$ comparing with $\theta_{1,2,3} = 0^\circ$ for considered Re_a range. The average estimated error between the numerical and experimental results, at certain Re_a, doesn't exceed 9 %. These results could be attributed to the fact that the overall drag consists of two combined parts, one presents the pressure drag while the other presents the friction drag. At the lower

Re_a, the friction drag is more dominant than the pressure drag leading to higher pressure drop while the opposite is true at the higher Re_a. In the case of high Re_a, the effect of the viscosity is less dominant and the total drag is rather affected by the inertia force. As the flow tend to shift more turbulent region, the separation point also travels farther downstream, reducing the size of the wake and the magnitude of the pressure drag.

Figure (16) shows the experimental P_{dc} versus $\theta_{1,2,3}$ at different Re_a. At a certain Re_a, P_{dc} increases with the angle of attack for $(0^\circ \leq \theta_{1,2,3} \leq 45^\circ)$ and $(180^\circ \leq \theta_{1,2,3} \leq 225^\circ)$, while P_{dc} decreases with the angle of attack for $(135^\circ \leq \theta_{1,2,3} \leq 180^\circ)$ and from 315° to 330°. At certain Re_a, for the angle of attack $\theta_{1,2,3} = 0^\circ$, and 30° the P_{dc} is about 87 % and 59 % lower than that of $\theta_{1,2,3} = 45^\circ$, respectively. The increase in P_{dc} at higher angles of attack is due to the increase of the airflow resistance.

Correlation for (P_{dc}) was predicted based on the experimental results obtained for various $\theta_{1,2,3}$ and at $1.8 \times 10^3 \leq Re_a \leq 9.7 \times 10^3$, with a maximum deviation of $\approx \pm 13$ %. The general form of the correlation is:

$$P_{dc} = a + b.(Re_a) + c.(1 + \frac{\theta^\circ}{90^\circ}) + d.(Re_a)^2 + e.(1 + \frac{\theta^\circ}{90^\circ})^2$$
$$+ f.(Re_a).(1 + \frac{\theta^\circ}{90^\circ}) \tag{7}$$

All constants of this correlation are listed in table (3).

4.2.2 Second and third cases of arrangements

Figure (17) shows the effect of Re_a on P_{dc} for case 2 and 3. In both cases, the values of P_{dc} decrease with Re_a increasing. As the total drag is a combination of friction and pressure drag, the values of P_{dc} are slightly higher and possibly dictated by the friction drag in the range of $1.8 \times 10^3 \leq Re_a \leq 4 \times 10^3$ for the arrangement of $(\theta_1 = 45^\circ, \theta_2 = 0^\circ, \theta_3 = 45^\circ)$. With an increase in Re_a, the relative influence of viscous forces decreases while that of the inertial forces increases. As seen from the figure (17a), the highest and lowest values of P_{dc} are obtained for the arrangements of $(\theta_1 = 45^\circ, \theta_2 = 0^\circ, \theta_3 = 45^\circ)$ and $(\theta_1 = 45^\circ, \theta_2 = 0^\circ, \theta_3 = 0^\circ)$, respectively. The values of P_{dc} for the arrangements of $(\theta_1 = 45^\circ, \theta_2 = 0^\circ, \theta_3 = 0^\circ)$ are 49 % lower, in average, than these for the arrangement of $(\theta_1 = 45^\circ,$

$\theta_2 = 0^\circ, \theta_3 = 45^\circ)$. On the other hand, for case 3, the highest value of P_{dc} is obtained for the arrangement $(\phi_1 = 90^\circ, \phi_2 = 90^\circ, \phi_3 = 90^\circ)$ at $Re_a = 1.8 \times 10^3$ while the lowest one is obtained for the arrangement $(\phi_1 = 90^\circ, \theta_2 = 0^\circ, \theta_3 = 0^\circ)$ at $Re_a = 9.7 \times 10^3$. For the arrangements of $(\phi_1 = 90^\circ, \theta_2 = 0^\circ, \phi_3 = 90^\circ)$, and $(\phi_1 = 90^\circ, \theta_2 = 0^\circ, \theta_3 = 0^\circ)$ the values of P_{dc} are lower by about 33 % and 63 % than these for $(\phi_1 = 90^\circ, \phi_2 = 90^\circ, \phi_3 = 90^\circ)$, respectively.

The best fit correlations obtained for P_{dc} and Re_a with the arrangements of $(\theta_1 = 45^\circ, \theta_2 = 0^\circ, \theta_3 = 45^\circ)$, and $(\phi_1 = 90^\circ, \phi_2 = 90^\circ, \phi_3 = 90^\circ)$ are:

$$P_{dc} = 49.47(Re_a)^{-0.27}, \quad R^2 = 0.983$$
$$1.8 \times 10^3 \leq Re_a \leq 9.7 \times 10^3, \theta_1 = 45^\circ, \theta_2 = 0^\circ, \theta_3 = 45^\circ \tag{8}$$

$$P_{dc} = 41.09(Re_a)^{-0.16}, \quad R^2 = 0.973$$
$$1.8 \times 10^3 \leq Re_a \leq 9.7 \times 10^3, \quad \phi_1 = \phi_2 = \phi_3 \tag{9}$$

4.3. Selection of Best Arrangement for Lowest Pumping Power

4.3.1 First case of numerical and experimental study

One of the goals of this study was to predict the optimal angle of attack that would minimize the frictional losses of the flow. A typical plot is provided to compromise between the angle of attack and the pumping power. A relationship (10) was obtained on multiplying the pressure drop and the volumetric flow rate as:

$$pumping\ power = \Delta P_a \cdot FR_{a,i} \tag{10}$$

where,

ΔP_a : Pressure drop, Pa

$FR_{a,i}$: Air volume flow rate, m³/s

Figure (18) shows the effect of the angle of attack $(\theta_{1,2,3})$ on the pumping power at different Re_a. At a certain Re_a, the pumping power increases with the angle of attack increasing from $(0^\circ$ to $45^\circ)$, and from $(180^\circ$ to $225^\circ)$ and decreases with the angle of attack increasing from $(135^\circ$ to $180^\circ)$ and from $(315^\circ$ to $330^\circ)$. The figure shows, also, that the lowest values of the pumping power are achieved at $\theta_{1,2,3} = 0^\circ$ for the considered Re_a range.

AIR FLOW CHARACTERISTICS OF STAGGERED WING-SHAPED TUBE BUNDLE AT DIFFERENT ANGLES OF ATTACK.
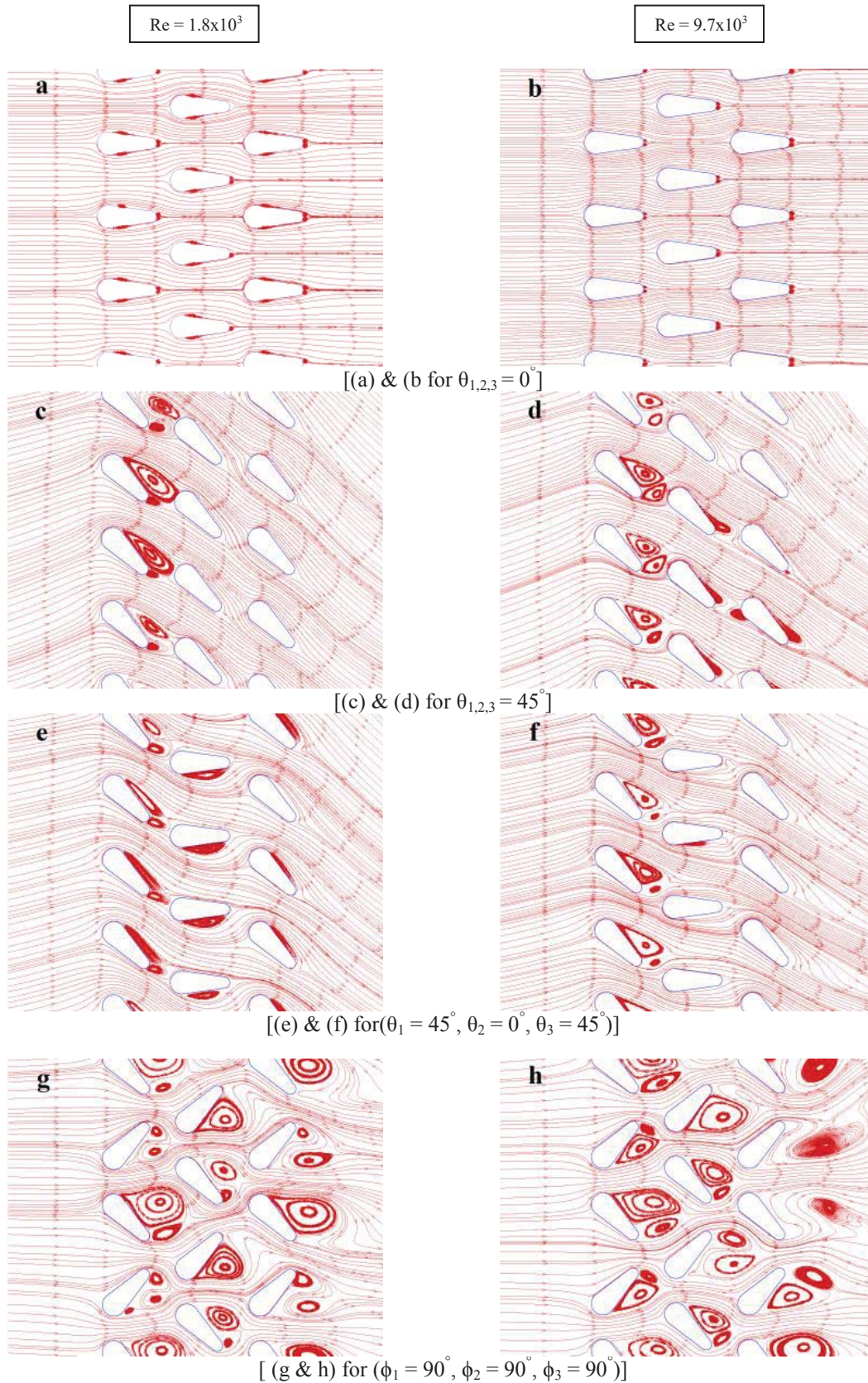*Sayed, Ibrahiem, Mesalhy, Abdulatief*

EIJEST

$Re = 1.8 \times 10^3$

$Re = 9.7 \times 10^3$

[(a) & (b for $\theta_{1,2,3} = 0°$]

[(c) & (d) for $\theta_{1,2,3} = 45°$]

[(e) & (f) for($\theta_1 = 45°$, $\theta_2 = 0°$, $\theta_3 = 45°$)]

[(g & h) for ($\phi_1 = 90°$, $\phi_2 = 90°$, $\phi_3 = 90°$)]

Figure 11 : Air Flow Path Lines of The Wing-Shaped Tubes of The Bundle at Different Angle Of Attack Arrangements.
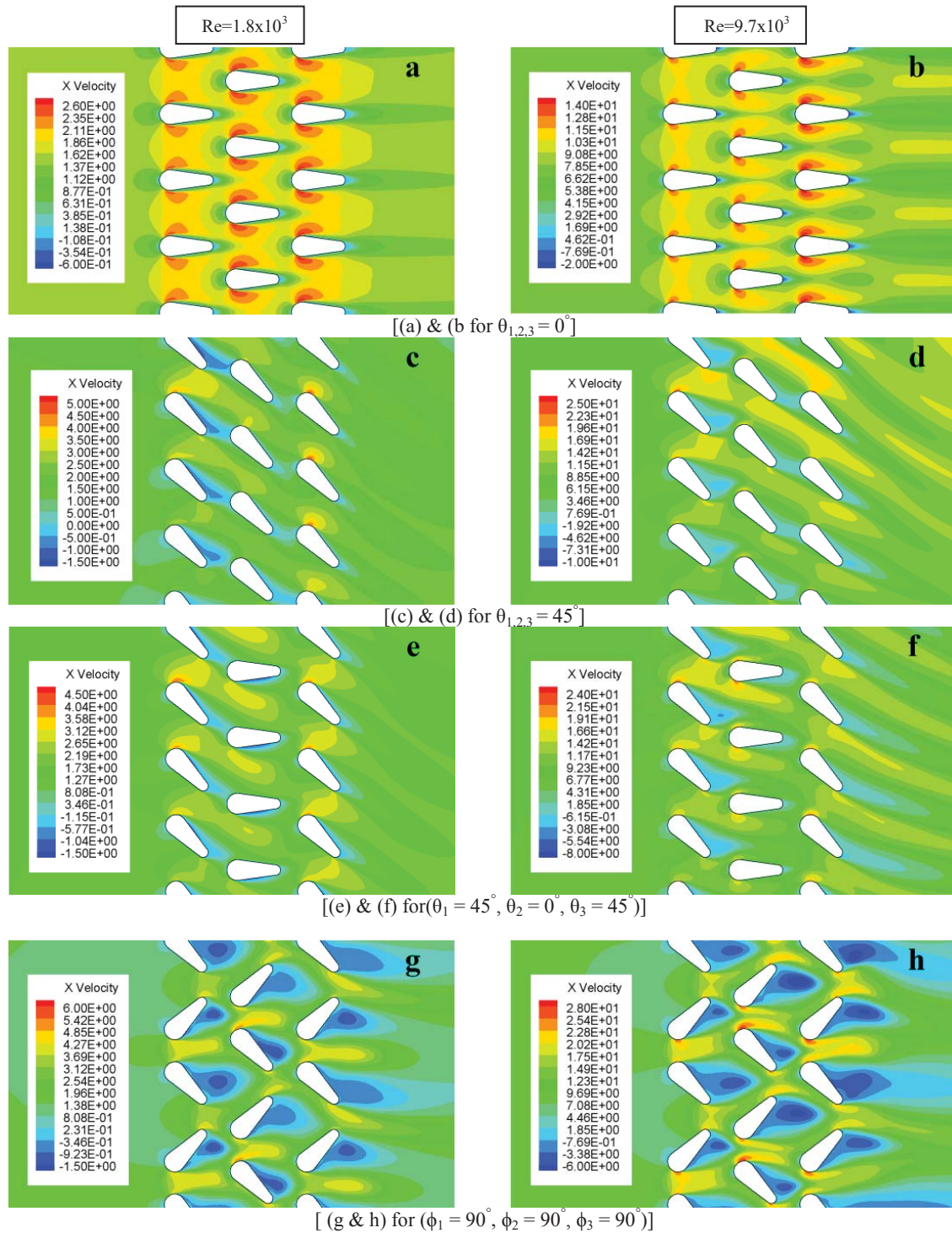
Figure 12 : Velocity Contours for Different Arrangements.

4.3.2 Second and third cases of arrangements

Figure (19) shows the effect of Re_a on the pumping power for cases (2) and (3). The pumping power increases with the increase of Re_a for all arrangements of case (2) and (3). The arrangement of $[\theta_1=45°, \theta_2=0°, \theta_3=45°]$ has higher pumping power value than that of the arrangement with $[\theta_1=45°, \theta_2=0°, \theta_3=0°]$ for case (2) for considered Re_a range. The arrangement with $[\phi_1=90°, \phi_2=90°, \phi_3=90°]$ for case (3) gives the highest value of pumping power in comparison with all arrangements of case (2) and (3). This

AIR FLOW CHARACTERISTICS OF STAGGERED WING-SHAPED TUBE BUNDLE AT DIFFERENT ANGLES OF ATTACK.
Sayed, Ibrahiem, Mesalhy, Abdulatief

EIJEST

is due to the fact that, the wing-shaped tubes bundle arrangement promoted turbulent mixing and lengthened the air flow-path through the bundle. The size and the strength of the turbulence level, as well as the reversed flow region are affected by θ, ϕ and Re_a variations.
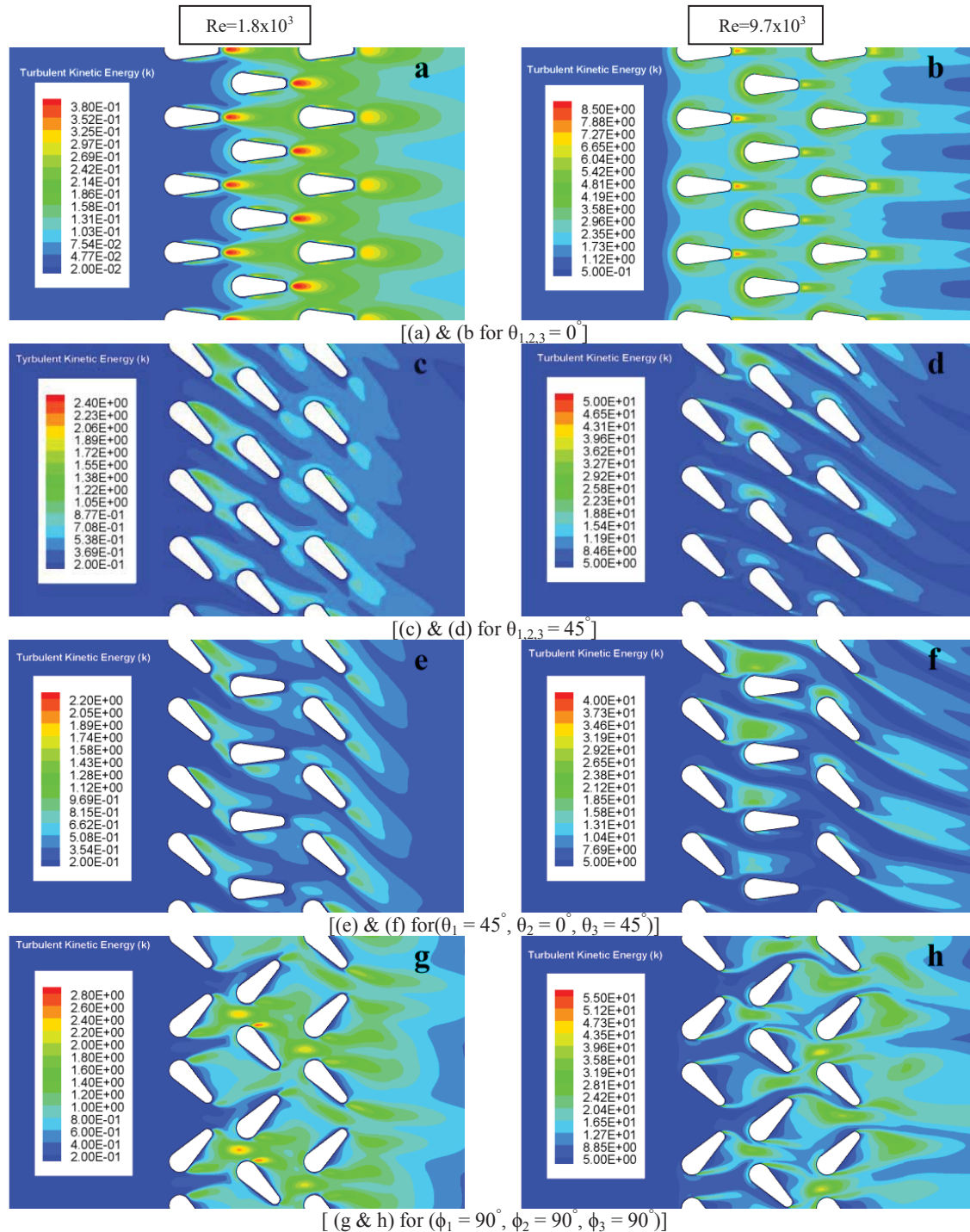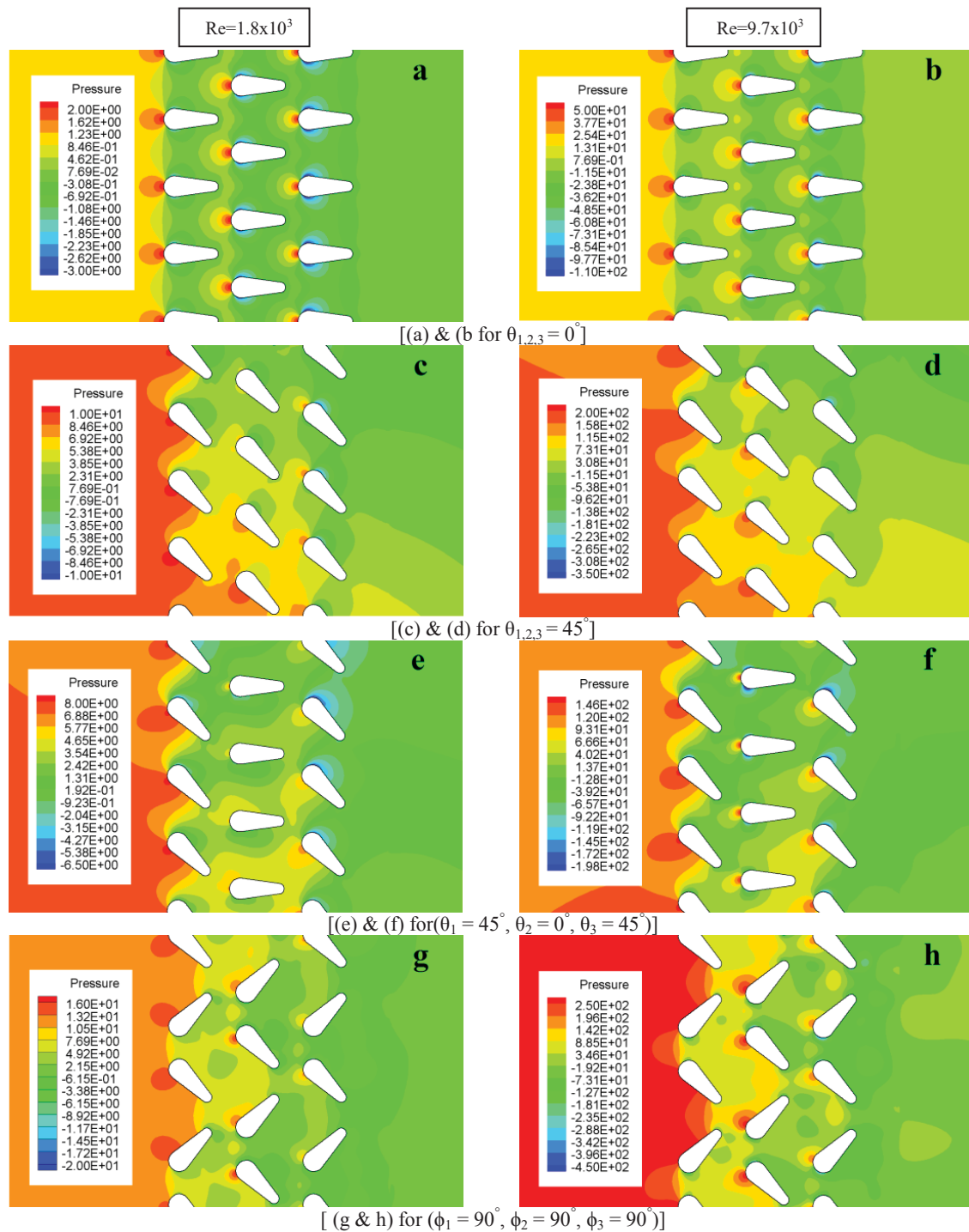

Figure 13 : Turbulent Kinetic Energy Contours for Different Arrangements.

Re=1.8x10³   Re=9.7x10³

[(a) & (b for $\theta_{1,2,3} = 0°$]

[(c) & (d) for $\theta_{1,2,3} = 45°$]

[(e) & (f) for($\theta_1 = 45°$, $\theta_2 = 0°$, $\theta_3 = 45°$)]

[(g & h) for ($\phi_1 = 90°$, $\phi_2 = 90°$, $\phi_3 = 90°$)]

Figure 14 : Static Pressure Contours Through The Bundle at Different Arrangements.

4.4 Comparison of Pressure Drop Coefficient and Pumping Power Results with Literature

The correlation of P_{dc} obtained in the present study

(Eq.7), was in a good agreement with that of (Eq.11) obtained by Sayed Ahmed et al. [8].

$$P_{dc} = 6.731 Re_a^{-0.238}, \quad R^2 = 0.97 \tag{11}$$

The deviation between the two correlations did not exceeded 6 %.

AIR FLOW CHARACTERISTICS OF STAGGERED WING-SHAPED
TUBE BUNDLE AT DIFFERENT ANGLES OF ATTACK.
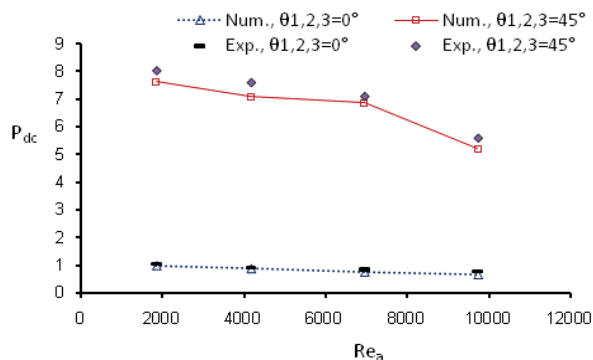*Sayed, Ibrahiem, Mesalhy, Abdulatief*

EIJEST

(a) Numerical

Figure 16 : Experimental P_{dc} versus $\theta_{1,2,3}$ at different Re_a.

(b) Experimental

$$P_{dc} = 49.47\, Re^{-0.27}$$
$$R^2 = 0.983$$
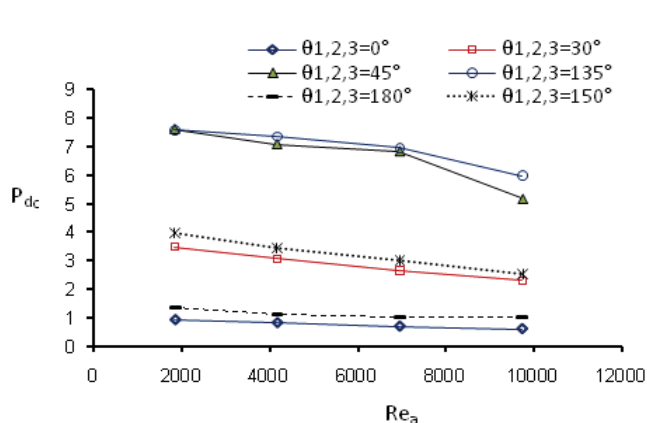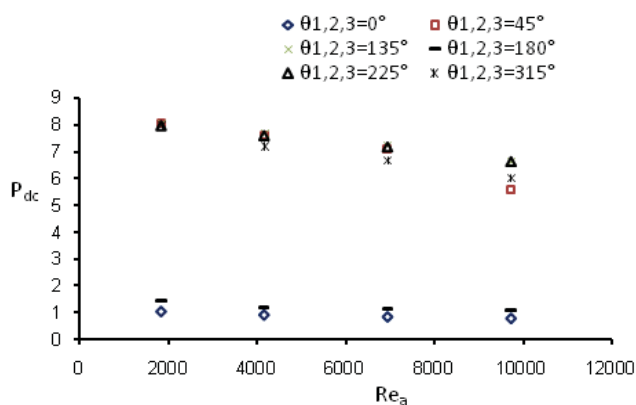
(a) Case 2

(c)Exp.-Num. validation

Figure 15 : Validation of Numerical and Experimental P_{dc}
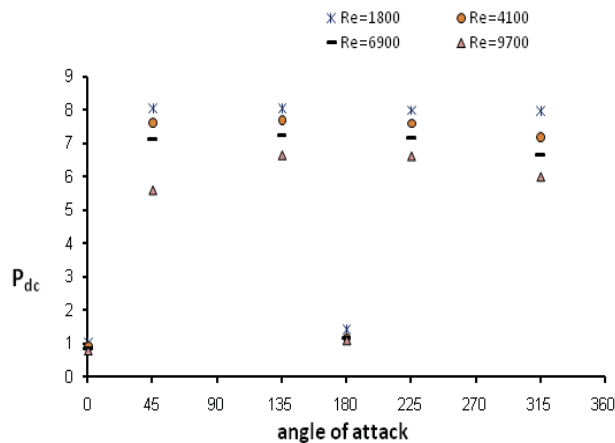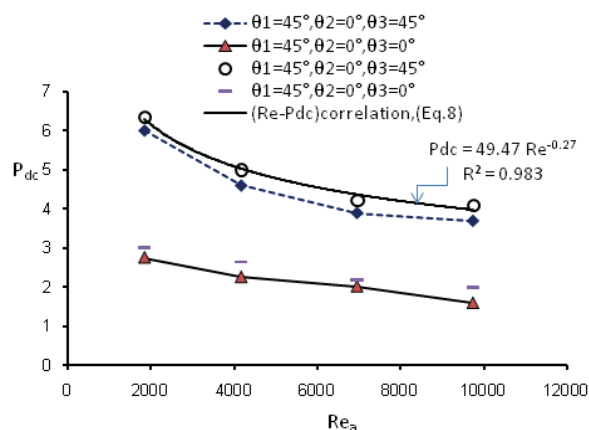Versus Re_a at Different $\theta_{1,2,3}$.

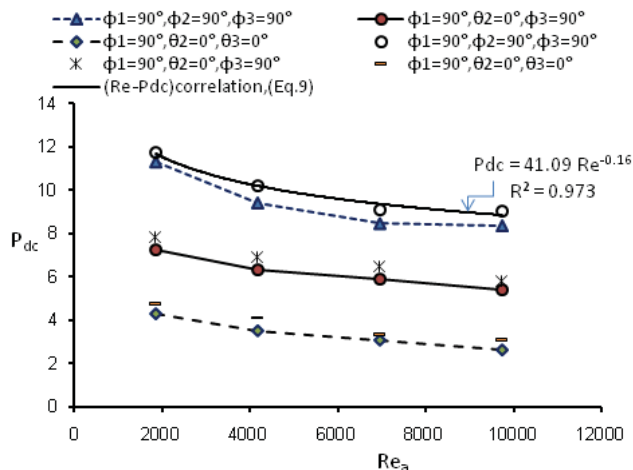$$P_{dc} = 41.09\, Re^{-0.16}$$
$$R^2 = 0.973$$

(b) Case 3

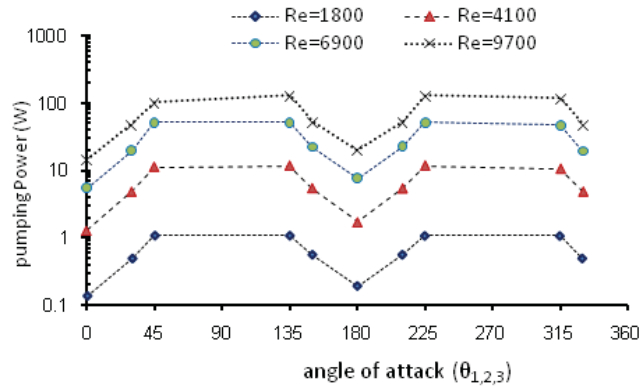**Figure 17:** The effect of Re_a on P_{dc} for Cases (2 and 3).

Figure 18 : Effect of Angle of Attack (θ) on Pumping Power (W) at Different Re_a

Table (3): Constants for Correlation (7).

a	b	c	d	e	f
$0^\circ \leq \theta_{1,2,3} \leq 45^\circ$, R^2=0.994					
40.2381	4.957×10^{-4}	-75.3	-7.778×10^{-9}	36.1	-4.6244×10^{-4}
$135^\circ \leq \theta_{1,2,3} \leq 180^\circ$, R^2=0.998					
329.14	-9.833×10^{-4}	-223.18	-9.702×10^{-11}	37.99	3.123×10^{-4}
$180^\circ \leq \theta_{1,2,3} \leq 225^\circ$, R^2=0.998					
342.94	7.7184×10^{-4}	-223.207	2.957×10^{-9}	36.472	-2.849×10^{-4}
$315^\circ \leq \theta_{1,2,3} \leq 360^\circ$, R^2=0.996					
879.219	-2.687×10^{-3}	-354.3082	-2.678×10^{-9}	35.7304	5.398×10^{-4}

The obtained correlation (Eq.7) was also compared with these obtained by Zukauskas [11] (Eq.12) and Ibrahim and Gomma [6] (Eq.13) by applying the conditions of the present study and using Re_a based on D_{eq}.

$$P_{dc} = 8.16 \, Re_a^{-0.207} \quad (1000 \leq Re_a \leq 20 \times 10^5) \tag{12}$$

$$P_{dc} = 1.17 \, Re_a^{-0.0466} \, (\sin(\alpha+10))^{0.052} \quad , \, (5300 \leq Re_a \leq 28000) \tag{13}$$
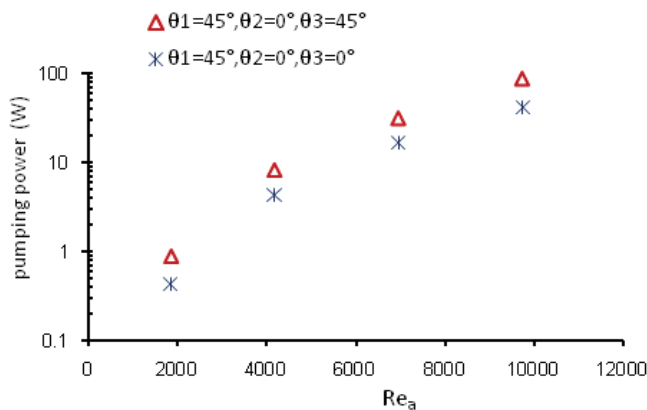
Figure (20) shows the comparison between the present study P_{dc} correlation and these obtained by the above mentioned authors for P_{dc}. It is clear from the figure, that the values of P_{dc} of the present study at $\theta_{1,2,3} = 0^\circ$ are, in average, lower than those obtained for the bundle of circular ones and higher than those obtained for the bundle with elliptical ones by about 36 % and 20 %, respectively for the considered Re_a range. The values of P_{dc} for the bundle of elliptical tubes with $\theta_{1,2,3} = 45^\circ$ are lower than those obtained for the present study, by about 88 % in average.

Figure (20c) shows that the highest values of P_{dc} are occurred for the arrangement of $[(\phi_1= 90^\circ, \phi_2= 90^\circ, \phi_3= 90^\circ)]$
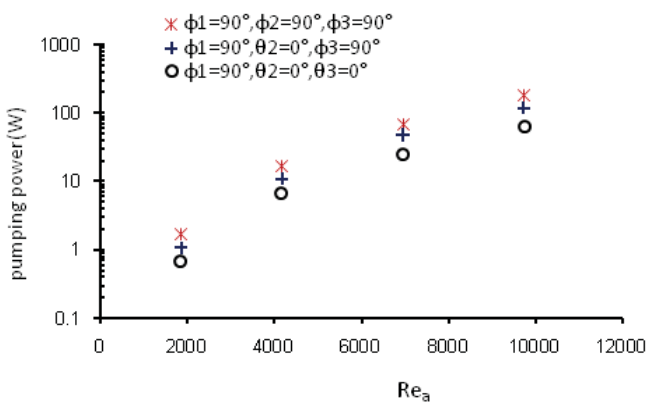
followed by the arrangements of ($\theta_{1,2,3} = 45^\circ$), ($\theta_1$=45°, θ_2=0°, θ_3=45°), and ($\theta_{1,2,3} = 0^\circ$). The values of P_{dc} for the arrangements of ($\theta_{1,2,3} = 45^\circ$), ($\theta_1$= 45°, θ_2= 0°, θ_3= 45°), and ($\theta_{1,2,3} = 0^\circ$) are lower than those of arrangement [ϕ_1=90°, ϕ_2=90°, ϕ_3=90°] by about 33%, 53%, and 91%,

respectively. Figure (21) shows that the highest values of pumping power are achieved for the arrangement of [(ϕ_1= 90°, ϕ_2= 90°, ϕ_3= 90°)] followed by the arrangements of ($\theta_{1,2,3} = 45^\circ$), ($\theta_1$=45°, θ_2=0°, θ_3=45°), and ($\theta_{1,2,3} = 0^\circ$) for the considered Re_a range.

The low resistance to the flow that the bundle of wing-shaped tubes offers is attributed to the tubes shapes. The streamlined shape of the wing-shaped tube provides smaller frontal area than that of circular one. This can be attributed to the better aerodynamic shape of the wing shaped tube leading to less drag forces. This enables the boundary layer to travel further along with the tube lateral surfaces before separation occurrence. It is suggested that an appropriate arrangement of the wing shaped tubes is required to obtain better global performance.

AIR FLOW CHARACTERISTICS OF STAGGERED WING-SHAPED TUBE BUNDLE AT DIFFERENT ANGLES OF ATTACK.
Sayed, Ibrahiem, Mesalhy, Abdulatief

EIJEST

(a) Case (2)

(a)

(b) Case (3)

Figure 19 : Effect of Re_a on Pumping Power for Cases (2 and 3).


(b)

5. CONCLUSIONS

Fluid flow characteristics and pressure drop distributions of wing-shaped tubes bundle placed in cross-flow have been numerically and experimentally investigated for $1.8 \times 10^3 \leq Re_a \leq 9.7 \times 10^3$. Three cases of the tubes arrangements were studied. Also, the commercial CFD software FLUENT 6.3.26 was utilized to predict the flow field around the wing-shaped tubes bundle. Flow path lines, velocity contours, turbulent kinetic energy contours, and static pressure contours were conducted to investigate the effect of different parameters on the fluid flow characteristics. Comparisons between the experimental and numerical results of the present study and those, previously, obtained for similar available studies showed agreements. The following conclusions are proffered:
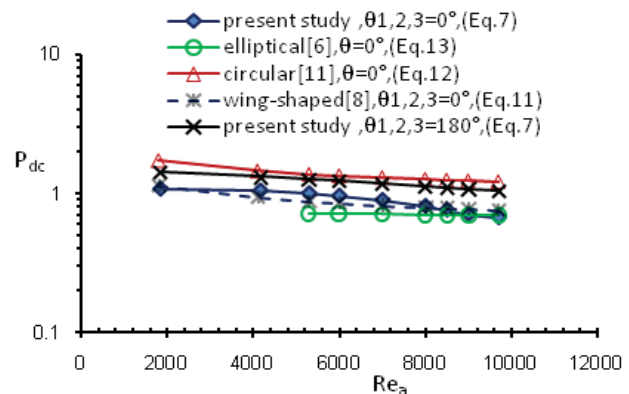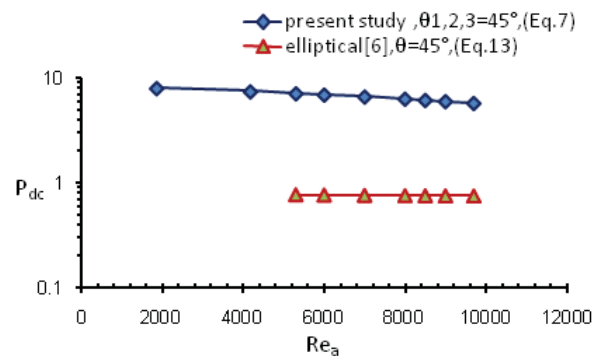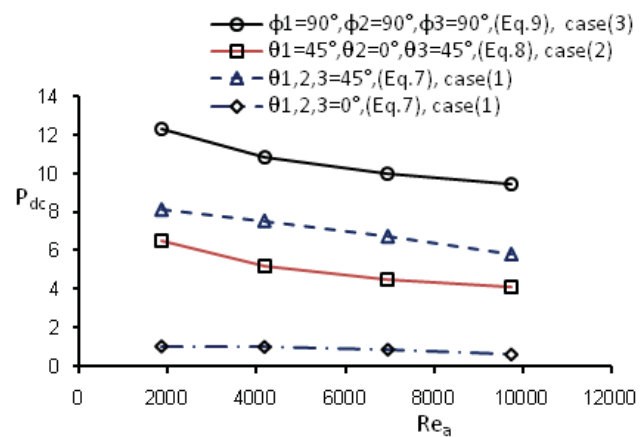
(c)

Figure 20 : Effect of Re_a on P_{dc} for The Bundles with Different Tubes Shapes and Angles of Attack.
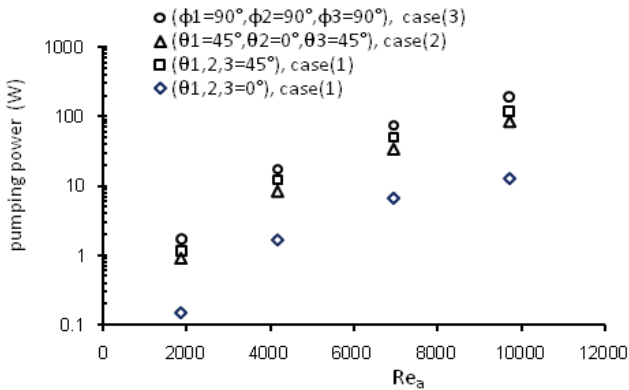
EIJEST

Figure 21 : Effect of Re_a on Pumping Power for Different Arrangements of the Present Study.

5.1. For First Case:

1. The dimensionless air flow pressure drop coefficient P_{dc} across the bundle decreased with increasing Re_a for all arrangements at a certain $\theta_{1,2,3}$.
2. The P_{dc} was found to be varied with Re_a in an inverse power law manner. A correlation of P_{dc} for the bundle of wing-shaped tubes with various $\theta_{1,2,3}$ and $1.8 \times 10^3 \leq Re_a \leq 9.7 \times 10^3$ was obtained.
3. The highest and the lowest values of P_{dc} were occurred for arrangements of $\theta_{1,2,3} = 45°, 135°, 225°, 315°$ and $\theta_{1,2,3} = 0°, 180°$, respectively.
4. At a certain Re_a, the P_{dc} and the pumping power increased with the angle of attack for $(0° \leq \theta_{1,2,3} \leq 45°)$ and $(180° \leq \theta_{1,2,3} \leq 225°)$, while decreased with the angle of attack for $(135° \leq \theta_{1,2,3} \leq 180°)$ and from $315°$ to $330°$. The lowest values of P_{dc} and pumping power were achieved at $\theta_{1,2,3} = 0°$ for all values of Re_a.
5. The values of P_{dc} for the wing-shaped tubes bundle at $\theta_{1,2,3} = 0°$ were, in average, lower than those obtained for the bundle of circular ones and higher than those obtained for the bundle with elliptical ones by about 36% and 20 %, respectively.
6. The values of P_{dc} for the bundle of elliptical tubes with $\theta_{1,2,3} = 45°$ are lower than those obtained for the present study, by about 88 % in average.

5.2. For Second and Third Cases:

The highest values of P_{dc} and pumping power were obtained for the arrangements of $(\theta_1=45°, \theta_2=0°, \theta_3=45°)$ and $(\phi_1=\phi_2=\phi_3=90°)$ for case 2 and 3, respectively. while, the arrangement with $[\phi_1=90°, \phi_2=90°, \phi_3=90°]$ for case (3) gave the highest values of P_{dc} and pumping power in comparison with all arrangements of the present study.

5.3. For All Cases:

The values of P_{dc} for the arrangements of $(\theta_{1,2,3} = 45°)$, $(\theta_1= 45°, \theta_2= 0°, \theta_3= 45°)$, and $(\theta_{1,2,3} = 0°)$ were lower than those for the arrangement of $[\phi_1=\phi_2=\phi_3=90°]$ by about 33%, 53%, and 91%, respectively.

REFERENCES

1.   Zhukauskas, A., and Ulinskas, R. V., [1985] " Efficiency parameters of heat transfer in tube banks", Heat Transfer Engineering, Vol.6, No.1, PP.19-25.

2.   Brauer, H., [1964] " Compact heat exchangers", J. Chem. Process Eng, pp. 451-460.

3.   Horvat, A., Leskovar, M. and Mavko, B., [2006] " Comparison of heat transfer conditions in tube bundle cross-flow for different tube shapes", International Journal of Heat and Mass Transfer, Vol. 49, pp. 1027-1038.

4.   Nishiyama, H., Ota, T., and Matsuno, t., [1988] " Heat transfer and flow around elliptic cylinders in tandem arrangement", JASME International Journal, Series II, Vol. 31, No. 3, pp. 410-419.

5.   Harris, D. K. and Goldschmidt, V. W., [2002] " Measurement of the overall heat transfer for combustion gases confined within elliptical tube heat exchangers", Experimental Thermal and Fluid Science, Vol. 26, pp. 33-37.

6.   Ibrahim, T. A., and Gomma, A., [2009] " Thermal performance criteria of elliptic tube bundle in cross flow", International Journal of Thermal Sciences, Vol. 48, PP. 1-11.

7.   Ibrahiem, E. Z., Elsyed, A. O., Sayed Ahmed, S. E., [2003] " Experimental investigation of the performance of a cross flow heat exchanger with bundle of semi-circular tubes", Mansoura Engineering Journal (MEJ), Vol.28, No.2.

8.   Sayed Ahmed, S. E., Mesalhy, O. M., Khass, T. M., and Hassan, A. H., [2012] " Parametric study of air cooling process via water cooled bundle of wing-shaped tubes" EIJST, Vol. 15, No. 3, pp. 1172-1184.

9.   Cengel, Y. A., [1998] " Heat transfer a practical approach, McGraw- Hill, New Jersey.

10.   FLUENT 6.3 User's Guide, [2006], FLUENT Inc.

11.   Zukauskas, A, [1972] " Heat transfer from tubes in cross flow in Advances in Heat Transfer" Edited by Hartnett, J. P. and Irvine, T. F. Jr, New York: Academic Press. Vol. 8, pp. 93-160.